

**This manuscript is a preprint** which has been submitted for publication.

It has **not undergone peer review** yet.

Subsequent versions of this manuscript may have slightly different content.

If accepted, the final version of this manuscript will be available via the 'Peer-reviewed Publication DOI' link on the right - hand side of this webpage.

Please feel free to contact any of the authors; we welcome feedback.

# Investigating global correlations between tsunami, earthquake, and subduction zone characteristics

I. van Zelst \*, S. Brizzi , E. van Rijsingen , F. Fucicello , Y. van Dinther 

<sup>1</sup>Seismology and Wave Physics, Institute of Geophysics, Department of Earth Sciences, ETH Zürich, Zürich, Switzerland, <sup>2</sup>Now at: Institute of Planetary Research, German Aerospace Center (DLR), Berlin, Germany, <sup>3</sup>Laboratory of Experimental Tectonics, Dip. Scienze, Roma Tre University, Rome, Italy, <sup>4</sup>Laboratoire de Géologie, École Normale Supérieure, PSL Research University, CNRS-UMR 8538, Paris, France, <sup>5</sup>Géosciences Montpellier, CNRS, Montpellier University, Montpellier, France, <sup>6</sup>Department of Earth Sciences, Utrecht University, Utrecht, The Netherlands

Author contributions: *Conceptualization*: I. van Zelst. *Methodology*: I. van Zelst, S. Brizzi. *Data curation*: I. van Zelst, S. Brizzi, E. van Rijsingen. *Formal Analysis*: I. van Zelst. *Writing - original draft*: I. van Zelst. *Writing - Review & Editing*: I. van Zelst, S. Brizzi, E. van Rijsingen, F. Fucicello, Y. van Dinther. *Visualization*: I. van Zelst. *Supervision*: F. Fucicello, Y. van Dinther. *Funding acquisition*: F. Fucicello, Y. van Dinther.

**Abstract** Tsunamigenic earthquakes pose a large hazard in subduction zones, but it is currently unclear in which - if any - tectonic setting they preferentially occur. Here, we compile the global Subduction Nature & Interconnected Tsunamigenic earthquake Characteristics (SNITCH) database with parameters on subduction geometry and tectonics, megathrust seismicity, and tsunami characteristics of tsunamis caused by earthquakes in subduction zones. We first use a bivariate regression analysis to reveal correlations between the normalised number of tsunamigenic earthquakes and the megathrust seismicity and tectonic parameters characterising a subduction zone. Considering the scarcity of tsunami data, we then employ the more robust multivariate Fisher analysis on the tectonic parameters to see which combination of parameters best distinguishes subduction zone segments in which relatively many and few tsunamis occur. The most important parameters in these combinations are consistently the type of margin (i.e., erosional or accretionary), the trench-normal component of the subduction and convergence velocity, the amount of trench sediments and the roughness of the incoming plate. Our results therefore suggest that tsunamigenic earthquakes may be more prone to occur in tectonic settings where plates subduct relatively fast beneath a sediment-starved, erosional margin with a complex, shallow subduction interface, characterised by multiple faults and fractures.

**Samenvatting** Tsunamiopwekkende aardbevingen vormen een groot gevaar in subductiezones, maar het is momenteel onduidelijk in welke tektonische gebieden deze vaker voorkomen - als dat al zo is. In dit artikel stellen we de globale Subductie-Aard & Geassocieerde Tsunamigene Aardbevingskenmerken (SNITCH) verzameling van data samen met parameters betreffende regionale subductiegeometrie en -tektoniek, seismiciteit langs de grote overschuivingsbreuk in subductiezones en tsunamikenmerken van tsunami's die veroorzaakt zijn door aardbevingen in subductiezones. We beginnen met een bivariate regressieanalyse die correlaties aantoont tussen het genormaliseerde aantal tsunamiopwekkende aardbevingen en de seismiciteit en tektonische parameters van subductiezones. Gezien de geringe hoeveelheid tsunamidata, gebruiken we vervolgens de robuustere multivariate Fisher-analyse voor de tektonische parameters om te kijken welke combinatie van parameters het beste onderscheid maakt tussen subductiezones waarin relatief veel en weinig tsunami's voorkomen. De belangrijkste parameters in deze combinaties blijken het systeemtype (d.w.z. erosief of accretionair), de loodrechte component van de subductie- en convergentiesnelheid, de hoeveelheid sedimenten, en de ruwheid van de topografie van de binnenkomende aardschol te zijn. Onze resultaten suggereren daarom dat tsunamiopwekkende aardbevingen mogelijk vaker voorkomen in gebieden waar aardschollen relatief snel subduceren in een erosief systeem met weinig sedimenten en meerdere breuken.

\*Corresponding author: iris.vanzelst@dlr.de / iris.v.zelst@gmail.com

**Riassunto** I terremoti tsunamigenici rappresentano una grande fonte di rischio nelle zone di subduzione. Tuttavia, non è chiaro se questi avvengano preferenzialmente in specifici contesti tettonici. In questo lavoro, presentiamo il database globale *Subduction Nature & Interconnected Tsunamiogenic earthquake Characteristics* (SNITCH), che contiene i parametri relativi alla geometria e contesto tettonico delle zone di subduzione, sismicità della faglia di subduzione, e le caratteristiche di tsunami generati da terremoti nelle zone di subduzione. In primo luogo, utilizziamo un'analisi di regressione bivariata per evidenziare eventuali correlazioni tra il numero normalizzato di terremoti tsunamigenici, i terremoti della faglia di subduzione e i parametri tettonici che caratterizzano una zona di subduzione. In secondo luogo, utilizziamo l'analisi multivariata di Fisher per delineare la combinazione di parametri che meglio permette di distinguere tra segmenti delle zone di subduzione con relativamente tanti o pochi terremoti tsunamigenici. Questo studio suggerisce che i terremoti tsunamigenici avvengono preferenzialmente in contesti tettonici in cui la placca in subduzione subduce velocemente al di sotto di un margine relativamente privo di sedimenti e di natura erosionale, con una faglia di subduzione poco profonda e caratterizzata da multiple faglie e fratture.

**Non-technical summary** In subduction zones, one tectonic plate moves below the other. This movement is facilitated by earthquakes that occur between and around the interface of the two plates. Since subduction zones are typically overlain by water, the seafloor displacements that are associated with these earthquakes can cause tsunamis with devastating consequences. Although this risk is known, it is at present unknown if earthquakes that cause tsunamis (so-called 'tsunamiogenic earthquakes') occur in any specific region more often than in other regions. Here, we compile a database that contains information on the geometry and structure of, and seismicity and tsunamis occurring in subduction zones around the world. We then use different statistical methods to see if there are any correlations between the amount of tsunamiogenic earthquakes and certain subduction zone or seismicity parameters. Our results suggest that tsunamiogenic earthquakes happen more often in subduction zones where the subducting plate moves relatively fast below the other plate; there are not many sediments; erosional processes of the rocks play a larger role than accretionary processes; and the seafloor contains multiple faults.

## 1 Introduction

Tsunamiogenic earthquakes are defined as earthquakes that cause tsunamis and usually occur on thrust faults in subduction zones. In the past decades, tsunamiogenic earthquakes have greatly impacted society, with the most notable events being the 2004  $M_w$  9.1–9.3 Sumatra-Andaman earthquake and resulting Indian Ocean tsunami, and the 2011  $M_w$  9.0 Tōhoku-Oki earthquake and tsunami (e.g., Lay et al., 2005; Titov et al., 2005; Fujii et al., 2011; Ozawa et al., 2011). During these large events, the megathrust typically plays the most important role, as it provides the largest potential slip area, and is therefore capable of producing the largest earthquake with an accompanying tsunami. However, other faults than the megathrust, such as outer rise or splay faults, likely play an important role in tsunamiogenesis as well (e.g., Fukao, 1979; Sibuet et al., 2007; Waldhauser et al., 2012; von Huene et al., 2016; Fan et al., 2017; Sladen and Trevisan, 2018). Since these faults have steeper dips than the megathrust, they can accommodate more vertical displacements for similar amounts of slip (Wendt et al., 2009; Van Zelst et al., 2022). However, it is difficult to determine whether an earthquake ruptured along the megathrust or a splay fault, due to the uncertainty in earthquake and tsunami source localisation (Sibuet et al., 2007; Waldhauser et al., 2012).

Tsunami earthquakes are a subset of tsunamiogenic earthquakes (Satake and Tanioka, 1999; Satake, 2015). They are defined by their disproportionately large tsunami waves compared to their seismic waves (Kanamori, 1972a). Other characteristics of tsunami earthquakes include their slow rupture velocity and long rupture duration (Kanamori, 1972a). It is typically thought that they rupture the shallowest part of the subduction interface (Lay et al., 2012), where the rocks contain many fluids and are velocity-strengthening and compliant (Bilek and Lay, 1999; Faulkner et al., 2011; Sahakian et al., 2019). Since tsunami earthquakes could pose an even larger, unexpected hazard than regular tsunamiogenic earthquakes, studies have typically focused on the possible mechanisms behind tsunami earthquakes and which type of subduction setting might be more prone to produce them (Polet and Kanamori, 2000; Bilek and Lay, 2002; Geersen, 2019). Based on these studies, two subduction zone parameters in particular are associated with tsunami earthquakes: the amount of sediments at the trench and the roughness of the subducting plate.

Tsunami earthquakes are typically associated with sediment-starved, erosional margins, because these settings can sustain very shallow slip due to their shallow frictional regime (Polet and Kanamori, 2000; Bilek, 2010; Geersen, 2019). However, it has also been suggested that sediment-rich margins could promote several aspects typical for tsunami earthquakes. The lower rigidity and strength of sediments could for example facilitate the slow tsunami earthquake rupture (Polet and Kanamori, 2000). Similarly, the sudden uplift of sediments in the unconsolidated accretionary wedge, which is typically larger in accretionary margins with large amounts of trench sediments, during

an earthquake could account for large vertical displacements of the water column (Seno, 2002; Tanioka and Seno, 2001).

Generally, tsunami earthquakes are associated with rough incoming plates (Tanioka et al., 1997; Polet and Kanamori, 2000; Geersen, 2019; Wang and Lin, 2022). The degree of roughness of an incoming plate is defined by the size and distribution of topographic features, such as seamounts, horst and graben structures, and ridges. Observations of past tsunami earthquakes, such as the 1947 Offshore Poverty Bay and Tolaga Bay earthquakes, have shown that ruptures could be affected by seamounts (Bell et al., 2014). Most notably, it has been speculated that the low rupture velocities typically associated with tsunami earthquakes stem from rupture on a seamount (Bell et al., 2014). Other structural features on the incoming plate, such as subducting fracture zones and fault structures (Robinson et al., 2006; Jiang et al., 2022), ridges (Gahalaut et al., 2010), and megathrust geometry and dip (Jiang et al., 2022) have also been proposed to influence the rupture and velocity of earthquakes in subduction zones. Similarly, a buried megathrust (Carvajal et al., 2022), slip depth (Carvajal et al., 2022), and slab dip (Oryan and Buck, 2020) have been suggested as factors influencing the tsunamigenic potential of ruptures.

The observed relationship between tsunami earthquakes, the amount of trench sediments in a subduction zone, and incoming plate roughness appears to be contrary to the relationship observed for large ( $M_w > 8.5$ ) megathrust earthquakes. Large megathrust earthquakes are typically associated with a smooth incoming plate and a large trench sediment thickness (Ruff, 1989; Heuret et al., 2012; Wang and Bilek, 2014; Scholl et al., 2015; Brizzi et al., 2018; Van Rijnsingen et al., 2018). However, it is unclear how tsunamigenic earthquakes, which include both tsunami earthquakes and some large megathrust earthquakes, are affected by trench sediments and incoming plate roughness. A global assessment, including statistics on the relationship between tsunamigenic earthquakes and general subduction zone characteristics, is still missing.

Here, we combine a subduction zone characteristics and megathrust seismicity database with a tsunami database. For the first time, we provide a global overview of parameters playing a role in the tsunamigenic earthquake process. We investigate the relationships between tsunamigenic earthquakes, megathrust seismicity, and the tectonic setting of subduction zones. Using bi- and multivariate statistical analyses, we identify subduction zone characteristics associated with the occurrence of tsunamigenic earthquakes. We find that fast-converging systems where an oceanic plate subducts at a sediment-starved, erosional margin are more prone to produce tsunamigenic earthquakes.

## 2 The SNITCH database

We compile a database containing information on megathrust seismicity, seismogenic zone geometry, subduction zone tectonics, and tsunami events. We call this database the Subduction Nature & Interconnected Tsunamigenic earthquake Characteristics (SNITCH) database. The SNITCH database consists of two parts: SNITCH-SN is a subduction zone database containing data on subduction zones characteristics and megathrust seismicity presented in Heuret et al. (2011, 2012); Brizzi et al. (2018) and Lallemand et al. (2018). SNITCH-T consists of characteristics of tsunamis caused by earthquakes compiled from NOAA NGDC/WDS Global Historical Tsunami data (Global Historical Tsunami Database, Retrieved: February 1, 2019). In the following, we describe how we assembled the SNITCH database in detail.

### 2.1 SNITCH-SN: Subduction nature

We compile our subduction zone characteristics database from the database of Heuret et al. (2011), and its subsequent versions (Heuret et al., 2012; Brizzi et al., 2018). This database consists of 62 subduction zone segments (Fig. 1) derived from merging 505 subduction zone transects based on homogeneous megathrust seismicity, homogeneous seismogenic zone geometry, or rupture areas for  $M_w \geq 8.0$  earthquakes confined in a single segment.

In addition to the parameters in the database from Heuret et al. (2011), we include two new parameters that quantify the roughness of the seafloor of the incoming plate prior to subduction according to Lallemand et al. (2018): long (i.e., 80–100 km) and short (i.e., 12–20 km) wavelength roughness. These parameters serve as a proxy for the roughness on the subduction interface. The different wavelengths are sensitive to different styles of topographic features on the subducting plate. Short wavelength roughness is typically associated with small- and intermediate-sized seamounts. Long wavelength roughness typically relates to large seamounts, seamount chains, and oceanic ridges. To translate the data provided by Lallemand et al. (2018) to the format of the 62 subduction zone segments used here, we average the roughness values for all transects comprising one subduction segment. Our final SNITCH-SN database has 25 different parameters (Table 1).

We sort the SNITCH-SN parameters in three different categories to simplify the analysis: megathrust seismicity, geometric, and tectonic parameters. The megathrust seismicity parameters result from earthquake observations from the ISC-GEM Global Instrumental Earthquake (Storchak et al., 2013) and Centennial-Harvard CMT catalogues spanning from 1900 up to 2007 (see Heuret et al., 2011; Brizzi et al., 2018, for more details). The geometric parameters of the seismogenic zone are derived from megathrust seismicity from 1900 to 2007 according to Heuret et al. (2011) (Fig. 3a). Therefore, the geometric parameters only shed light on the geometry of the seismogenic zone along the megathrust and do not include information on the geometry of the downgoing slab, overriding plate, splay or outer rise faults.  $W_{\text{intraslab}}$  considers the entire downdip length of the slab and is derived from all intraslab earthquakes

**Table 1** Parameters in the SNITCH-SN database: subduction nature

Symbol	Parameter	Unit
Megathrust seismicity parameters		
$N_{eq}$	Number of earthquakes	-
$\tau$	Seismicity rate: number of events per century and per $10^3$ km trench	-
$CSM$	Cumulative seismic moment	N m
$M_{mrr}$	Equivalent representative magnitude in the sense of <a href="#">Ruff and Kanamori (1980)</a>	-
$M_{max,GEM1900}$	Maximum $M_w$ from 1900–2007 according to the ISC-GEM catalogue	-
$M_{max,Cent\&CMT}$	Maximum $M_w$ from 1900–2007 according to the Centennial & CMT catalogues	-
$M_{max,GEM1960}$	Maximum $M_w$ from 1960–2007 according to the ISC-GEM catalogue	-
Geometric parameters (based on seismicity)		
$z_{min}$	Depth of the updip limit of the seismogenic zone	km
$z_{max}$	Depth of the downdip limit of the seismogenic zone	km
$x_{min}$	Distance from the trench to the updip limit of the seismogenic zone	km
$x_{max}$	Distance from the trench to the downdip limit of the seismogenic zone	km
$W_{interplate}$	Downdip width of the seismogenic zone	km
$\theta$	Dip of the megathrust	°
$R$	Curvature radius of the slab at the trench	km
$W_{intraslab}$	Downdip length of the slab	km
Tectonic parameters		
$L^*$	Trench-parallel extent of the subduction zone segment	km
$A$	Age	Myr
$D_{arc-trench}$	Mean distance between the volcanic arc and the trench	km
UPS	Upper plate strain 1 = extension (E); 2 = neutral (N); 3 = compression (C)	-
$T_{sed}$	Sediment thickness at the trench	km
AvsE	Type of margin 0 = accretionary (A); 1 = erosional (E)	-
$R_{sw}$	Short wavelength roughness (12-20 km)	m
$R_{lw}$	Long wavelength roughness (80-100 km)	m
$v_{sn}$	Trench-normal component of the subduction velocity from <a href="#">DeMets et al. (1990)</a>	mm year <sup>-1</sup>
$v_{cn}$	Trench-normal component of the convergence velocity from <a href="#">DeMets et al. (1990)</a>	mm year <sup>-1</sup>

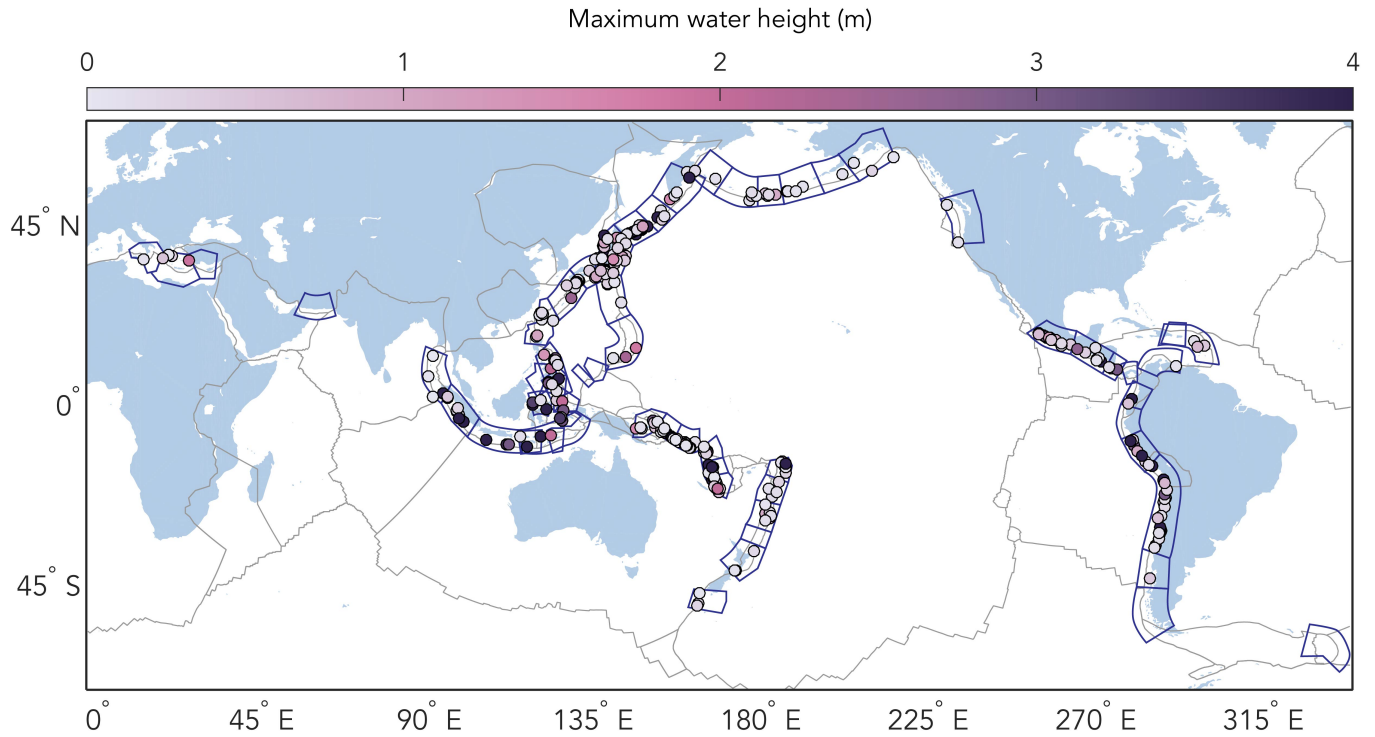


**Figure 1** All 329 definite tsunami events caused by an earthquake in the NOAA NGDC/WDS Global Historical Tsunami Database that occurred from 1962 to 2018, organised into the subduction zone segments (dark blue) defined by Heuret et al. (2011). Events are coloured by maximum observed water height.

recorded in the area. The tectonic parameters are independent of any earthquake catalogue, and give insight into the nature of the subducting and overriding plate, the large scale geometry of the system, such as the distance between the volcanic arc and the trench  $D_{\text{arc-trench}}$ , and the kinematics of the subduction zone.

## 2.2 SNITCH-T: Tsunamigenic earthquakes

We download data from the NOAA NGDC/WDS Global Historical Tsunami Database (Global Historical Tsunami Database, Retrieved: February 1, 2019) as the NOAA database is well suited for studying the statistics on the occurrence of tsunamis (Gusiakov et al., 2019). We select definite tsunami events that were caused by an earthquake from 1962–2018. We choose 1962 to start our data retrieval, because of the instalment of the World-Wide Standardised Seismograph Network that year, which ensured global monitoring of earthquakes. Prior to 1962, the NOAA NGDC/WDS Global Historical Tsunami Database is potentially incomplete which could skew our statistical analysis. Using the 1962–2018 time window, we extract 395 tsunamis. Note that due to this limited time window, large historical tsunamigenic earthquakes such as the 1944  $M_w$  8.0–8.3 Tonankai (Kanamori, 1972b), 1946  $M_w$  8.1–8.4 Nankaido (Kanamori, 1972b), 1946  $M_w$  7.4 Aleutian (López and Okal, 2006), and 1960  $M_w$  9.4–9.6 Chile (Kanamori and Cipar, 1974; Satake and Atwater,

**Table 2** Parameters in the SNITCH-T database: tsunamigenic earthquakes

Symbol	Parameter	Unit
$N_t$	Normalised number of tsunamis per km trench	-
$N_{t,\text{tot}}$	Total number of tsunamis in a subduction zone segment	-
$h_{w,\text{max}}$	Maximum water height observed for an event in a segment	m
$\bar{h}_w$	Average maximum water height of all events in a segment	m
$m_{t,\text{max}}$	Maximum tsunami magnitude observed for an event in a segment	-
$\bar{m}_t$	Average tsunami magnitude of all events in a segment	-
$I_{t,\text{max}}$	Maximum tsunami intensity observed for an event in a segment	-
$\bar{I}_t$	Average tsunami intensity of all events in a segment	-
$\bar{z}_f$	Average earthquake focal depth of all events in a segment	km
$z_{f,\text{min}}$	Minimum earthquake focal depth in a segment	km
$M_{w,\text{max}}$	Maximum earthquake magnitude in a segment	-
$\bar{M}_w$	Average earthquake magnitude of all events in a segment	-
$M_{w,\text{min}}$	Minimum earthquake magnitude in a segment	-

2007) earthquakes are not included in the SNITCH-T database. Because some of the parameters in the SNITCH-SN database are based on megathrust seismicity data up to 2007 (Sec. 2.1), we make a second version of the SNITCH-T database that is limited to 2007, which consists of 284 tsunamis. Hence, there are two versions of the SNITCH-T database: SNITCH-T-2007 and SNITCH-T-2018. Note that large recent tsunamigenic earthquakes such as the 2010  $M_w$  8.8 Maule (Delouis et al., 2010) and 2011  $M_w$  9.0 Tōhoku earthquakes (Fujii et al., 2011) are not part of the SNITCH-T-2007 database due to the applied time window.

For each tsunami in the NOAA NGDC/WDS Global Historical Tsunami Database, we extract the tsunami source location (i.e., earthquake epicenter), maximum water height measured  $h_w$ , tsunami magnitude  $m_t$ , tsunami intensity  $I_t$ , earthquake magnitude  $M_w$ , and earthquake hypocenter depth  $z_f$  (i.e., the focal depth).

The tsunami magnitude  $m_t$  is defined by Iida et al. (1967) as:

$$m_t = \log_2 h, \quad (1)$$

where  $h$  is the maximum runup height of the tsunami wave.

The tsunami intensity  $I_t$  is defined by (Soloviev and Go, 1974) as:

$$I_t = \log_2 (\sqrt{2} \cdot h). \quad (2)$$

We sort all tsunamis into the subduction zone segments defined by Heuret et al. (2011) based on their tsunami source location. For the SNITCH-T-2018 database, 66 events are situated outside the subduction zone segments. We remove these events from our analysis, as they are not associated with tsunamigenic earthquakes in subduction zones. This results in a total of 329 tsunamis in the SNITCH-T-2018 database (Fig. 1). In the SNITCH-T-2007 database, 47 tsunamis are situated outside the subduction zone segments, so the final SNITCH-T-2007 database consists of 237 tsunamis.

As the subduction zone segments consist of rectangular transects, they can overlap in some places. If a tsunami is placed in an area where two or more subduction zone segments overlap, we manually place it in a segment. For this purpose, we consider the depth of the earthquake, which better suggests with which subducting plate, and hence which subduction zone segment, a tsunami should be associated. In total, there are 46 tsunamis (14% of all tsunamis in SNITCH-T-2018) that are manually sorted into subduction zone segments according to their depth and the subduction geometry at depth (e.g., from tomographic studies).

When all tsunami events are sorted in a subduction zone segment, we count the amount of tsunamis in each subduction zone ( $N_{t,tot}$ ) and calculate the normalised number of tsunamis per km trench  $N_t$

$$N_t = \frac{N_{t,tot}/L^*}{\max(N_{t,tot}/L^*)}, \quad (3)$$

where  $L^*$  is the along-strike length of a subduction segment. For each segment, we also calculate the maximum water height  $h_{w,max}$  among all events that occurred in that segment, the average maximum water height observed for the events  $\bar{h}_w$ , the maximum and average tsunami magnitude  $m_t$  and intensity  $I_t$ , the average and minimum focal depth  $z_f$ , and the minimum, average, and maximum earthquake magnitude  $M_w$  that caused a tsunami in that segment. We then have 13 parameters in the SNITCH-T database (Table 2).

Considering the limited amount of data in the SNITCH-T database due to the short observational time window, it is useful to look at scale-free measures of tsunamigenesis. Similarly, as the data in the NOAA NGDC/WDS Global Historical Tsunami Database is scarce for each tsunami, some subduction segments do not have values for all parameters. The only parameters for which we have a complete record for all subduction zone segments are  $N_t$  and  $N_{t,tot}$ . As  $N_t$  is a normalised measure of tsunamigenesis independent of the size of the subduction segments, we deem  $N_t$  the most reliable quantity for robust insights on the relationship between tectonics and tsunamigenesis. Therefore, we focus our analysis on  $N_t$ .

### 3 Bivariate statistical analysis

#### 3.1 Methods

We calculate the Pearson's product-moment correlation coefficient  $R_p$  for SNITCH-T with itself and SNITCH-SN. The Pearson's product-moment correlation coefficient gives insight into the linear correlation between two variables. To reduce the effect of outliers on linear correlations, we also calculate the Spearman rank correlation coefficient  $\rho$ , in which the similarity or monotonicity between two variables is assessed, regardless of any linear relationship that might exist between them.

To focus our analysis, we consider a relationship between two variables worthy of further investigation if both the Pearson and Spearman correlations are higher than or equal to 0.3 (Heuret et al., 2011) with  $p$ -values smaller than 0.05 (i.e., there is less than a 5% chance that the null hypothesis of there being no correlation is true).  $p$ -values for the Spearman correlations are indicated by  $p$  and  $p$ -values for Pearson correlations are indicated by  $p_p$ . For visualising our results, we show the Spearman's rank correlation coefficient (Sec. 3.2), because it typically shows the highest

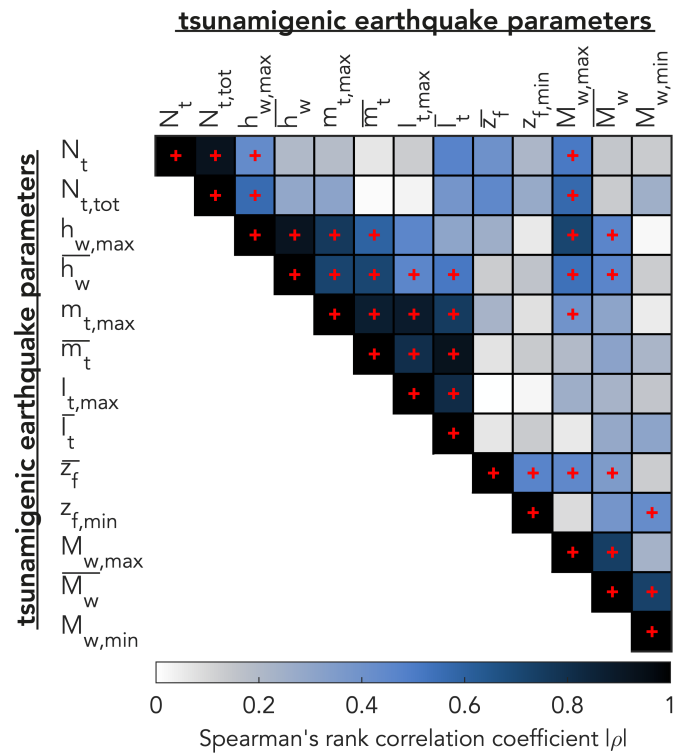


**Figure 2** Spearman's rank correlation coefficients for SNITCH-T-2018: tsunami and tsunamigenic earthquake characteristics correlated with itself. Significant positive and negative correlations worthy of further investigation as defined in Sec. 3.1 are indicated by a red plus and minus sign, respectively. Abbreviations for parameters are explained in Table 2.

221 correlations. This is due to the fact that the data is not linear, and can more easily be described by a monotonic  
 222 relationship. However, the differences in correlation coefficients between the two methods is on average only a  
 223 few percent. The results for Pearson's product-moment correlation coefficient can be found in the Supplementary  
 224 Material.

## 225 3.2 Results

### 226 3.2.1 Tsunamigenic earthquakes

227 Fig. 2 shows the correlation matrix for the Spearman's rank correlation coefficients of SNITCH-T-2018 with itself.  
 228 In this and the following figures, correlations that are significant under our definition in Sec. 3.1 are indicated by  
 229 a red plus or minus sign depending on a positive or negative correlation, respectively. Additional scatter plots and  
 230 numbers for the correlations and corresponding  $p$ -values can be found in the Supplementary Material.

231 The normalised number of tsunamis per km trench  $N_t$  and total number of tsunamis in a subduction zone seg-  
 232 ment  $N_{t,tot}$  correlate positively with the maximum water height  $h_{w,max}$  ( $\rho = 0.44$  and  $\rho = 0.56$ , respectively), which  
 233 relates to the fact that the likelihood of a tsunami with high maximum water height is larger when sufficient tsunami  
 234 events occur in a given subduction zone. A similar reasoning can be applied to the correlations between  $N_t$  and  $N_{t,tot}$   
 235 and  $M_{w,max}$  ( $\rho = 0.44$  and  $\rho = 0.49$ , respectively), as a large number of tsunamigenic earthquakes in a subduction zone  
 236 increases the likelihood of a big earthquake being the cause of such an event.

237 The maximum water height parameters and  $m_{t,max}$  also correlate positively with the maximum and average earth-  
 238 quake magnitude, which indicates that larger earthquakes produce larger wave heights and hence tsunami magni-  
 239 tudes and intensities.

240 The average focal depth of the tsunamigenic earthquakes correlates positively with the magnitude of the earth-  
 241 quake ( $\rho = 0.35$ ), indicating that a larger earthquake magnitude corresponds to a deeper focal depth. This is rein-  
 242 forced by the correlation between the shallowest focal depth and the minimum earthquake magnitude ( $\rho = 0.43$ ).  
 243 Hence, large tsunamigenic earthquakes likely nucleate at larger focal depths.

### 244 3.2.2 Megathrust seismicity

245 The Spearman's rank correlation coefficient matrix of the tsunamigenic earthquake parameters of SNITCH-T-2007  
 246 and the megathrust seismicity parameters of SNITCH-SN is shown in Fig. 3b.  $N_t$  correlates well with the number of  
 247 earthquakes  $N_{eq}$  ( $\rho = 0.57$ ), the seismicity rate  $\tau$  ( $\rho = 0.63$ ), and the various measures of the maximum earthquake  
 248 magnitude ( $0.34 < \rho < 0.46$ ). This indicates that more tsunamis are associated with subduction zone segments that



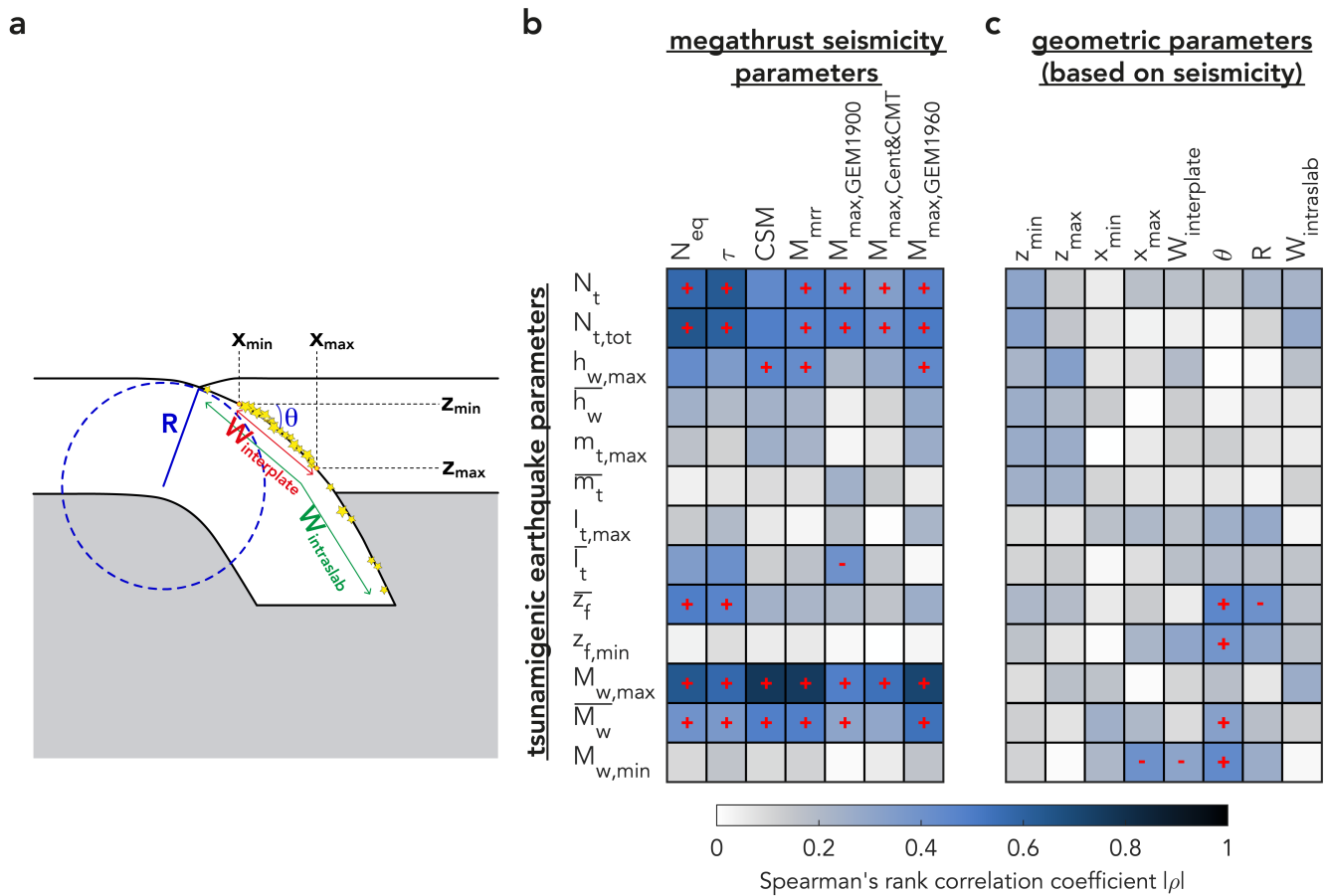


**Figure 3** (a) Diagram showing how the geometric parameters in the SNITCH-SN database are estimated based on the extent of megathrust seismicity (yellow stars). (b,c) Spearman's rank correlation coefficients for SNITCH-T-2007 correlated with (b) the megathrust seismicity and (c) the geometric parameters (based on seismicity) of SNITCH-SN. Significant positive and negative correlations worthy of further investigation as defined in Sec. 3.1 are indicated by a red plus and minus sign, respectively. Abbreviations for parameters are explained in Tables 1 and 2.

249 have experienced larger megathrust earthquakes. The maximum water height  $h_{w,max}$  correlates with some megathrust  
 250 seismicity parameters, such as the cumulative seismic moment  $CSM$  ( $\rho = 0.45$ ), and the equivalent representative  
 251 magnitude  $M_{mirr}$  ( $\rho = 0.43$ ). This indicates that larger wave heights are associated with larger earthquakes. The  
 252 maximum and average maximum magnitude of tsunamigenic earthquakes in a subduction zone correlate well with  
 253 all the megathrust seismicity measures ( $0.3 < \rho < 0.76$ ), with the exception of  $M_{max,Cent\&CMT}$  for  $\bar{M}_w$ .

### 254 3.2.3 Geometry of the seismogenic zone and slab

255 There are few correlations between the geometric parameters describing the seismogenic zone and subducting slab  
 256 in SNITCH-SN and the tsunamigenic earthquake parameters of SNITCH-T-2007 (Fig. 3a). The only significant correlations  
 257 are found between the dip of the subduction zone  $\theta$  and the average earthquake focal depth  $\bar{z}_f$  ( $\rho = 0.46$ ).  
 258 This indicates that a larger dip results in a larger focal depth, which is to be expected as a larger dip of a subducting  
 259 plate (i.e., a steeper slab) is often associated with a deeper seismogenic zone limit. The negative relationship between  
 260  $\bar{z}_f$  and the radius of curvature  $R$  ( $\rho = -0.40$ ) reflects the same physical explanation. The average and minimum  
 261 tsunamigenic earthquake magnitude also correlate positively with the dip of the subduction zone.

### 262 3.2.4 Tectonics of the subduction system

263 The tectonic parameters describe the large scale structure, geometry, kinematics, and nature of the subduction zone.  
 264 Since the tectonic parameters are not influenced by a limited observational time span, we correlate them with the  
 265 SNITCH-T-2018 database (Fig. 4).

266 We find a positive correlation between the type of margin  $AvsE$  and  $N_t$  ( $\rho = 0.35$ ), which translates to erosional  
 267 margins being associated more with tsunamigenic earthquakes. This is corroborated by the negative correlation  
 268 between  $N_t$  and  $T_{sed}$  ( $\rho = -0.40$ ).

269  $N_t$  correlates positively with the trench-normal component of the subduction and convergence velocity ( $v_{sn}$  and  
 270  $v_{cn}$ ;  $\rho = 0.66$  and  $\rho = 0.47$ , respectively), which complies with the assumption that more tsunamigenic earthquakes  
 271 would be recorded during the same time span in settings where the stress build-up is more rapid.

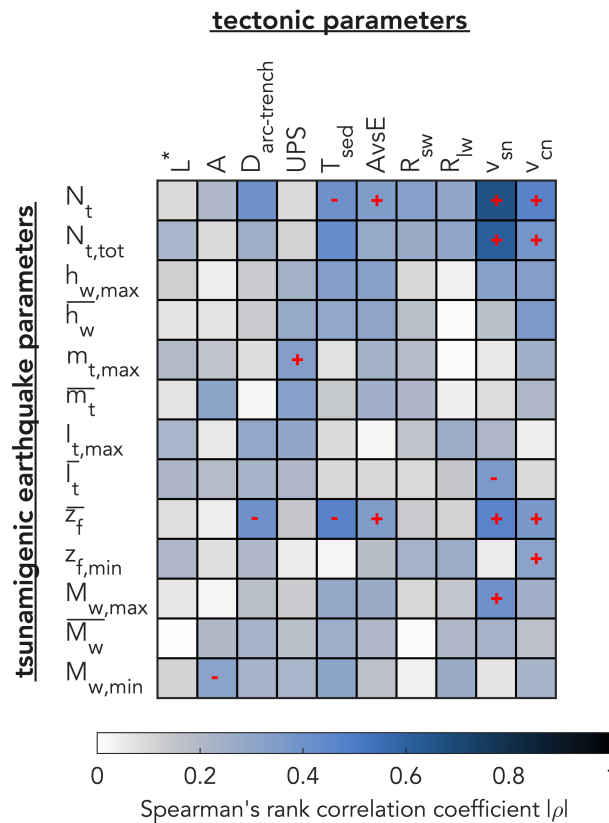


**Figure 4** Spearman's rank correlation coefficients for SNITCH-T-2018 correlated with tectonic parameters of SNITCH-SN. Significant positive and negative correlations worthy of further investigation as defined in Sec. 3.1 are indicated by a red plus and minus sign, respectively. Abbreviations for parameters are explained in Tables 1 and 2.

The maximum tsunami magnitude correlates positively ( $\rho = 0.33$ ) with the upper plate strain, meaning that compressional upper plates are more often associated with larger tsunami magnitudes. The average focal depth of tsunamigenic earthquakes  $\bar{z}_f$  shows a negative relationship with  $T_{sed}$  ( $\rho = -0.47$ ), and a positive correlation with  $AvsE$  ( $\rho = 0.35$ ), indicating erosional margins are more associated with a larger average focal depth.

The average focal depth also correlates with both velocity measures. In line with  $N_t$ , the maximum tsunamigenic earthquake magnitude  $m_{t,max}$  correlates with the trench-normal component of the subduction velocity  $v_{sn}$  ( $\rho = 0.40$ ).

Fig. 5 shows scatter plots of  $N_t$  versus the tectonic parameters (Table 1). There are trends visible between  $AvsE$ ,  $v_{sn}$ , and  $v_{cn}$  versus  $N_t$  as expected from the high correlations found by the Spearman and Pearson methods. Large  $N_t$  only occurs for low sediment thickness  $T_{sed}$ . There also seems to be a trend for both seafloor roughness parameters, indicating that a rougher seafloor is associated with more tsunamis. This is confirmed by the significant ( $p < 0.05$ ), relatively high ( $\rho = 0.32$  for  $R_{sw}$  and  $\rho = 0.30$  for  $R_{lw}$ ) Spearman rank correlations for both  $R_{sw}$  and  $R_{lw}$ , although no significant, high correlations are found for the Pearson's coefficient. The two subduction zone segments with the highest normalised number of tsunamis  $N_t$  are Japan and South-Kuril. Because of their high  $N_t$ , they are often outliers.

## 4 Multivariate statistical analysis

### 4.1 Methods

The bivariate analyses presented in Sec. 3 suffer from the scarcity of tsunami data. This is illustrated by the limited amount of significant correlation coefficients (i.e.,  $p < 0.05$ ) for both the Pearson's product-moment and the Spearman rank analyses. A multivariate approach, as described in this section, can help to further reveal the conditions promoting tsunamigenic earthquakes, despite the scarcity of the tsunami data.

Following Sandri et al. (2004) and Brizzi et al. (2018), we use the Fisher discriminant method (e.g., Duda et al., 1973) to perform a pattern recognition analysis focused at discovering combinations of parameters that could promote the occurrence of tsunamigenic earthquakes. We only consider the tectonic parameters of the SNITCH-SN database to take advantage of the larger amount of data in the corresponding SNITCH-T-2018 database. We exclude  $L^*$ , because this parameter solely depends on the choice of the subduction zone segments and does not represent a physical feature of the subduction system.

We first identify linear combinations that can divide the subduction zone segments in two classes based on  $N_t$ ,

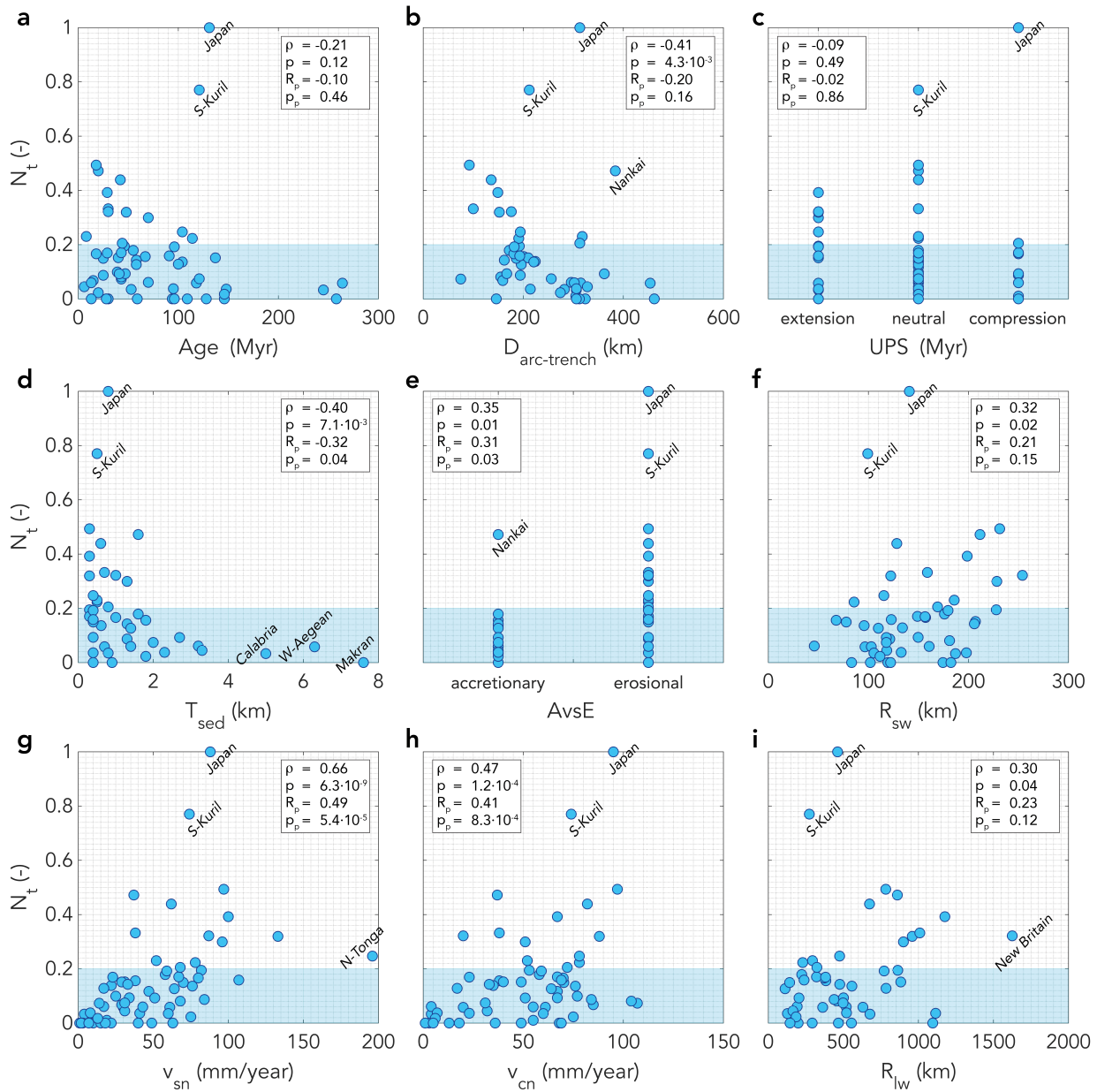


**Figure 5** Scatter plots showing the relation between the normalised number of tsunamigenic earthquakes per km trench  $N_t$  and (a) the age of the subducting plate  $A$ ; (b) the distance between the volcanic arc and the trench  $D_{arc-trench}$ ; (c) the upper plate strain  $UPS$ ; (d) the sediment thickness at the trench  $T_{sed}$ ; (e) the type of margin  $AvsE$ ; (f) the short wavelength (i.e., 12–20 km) roughness  $R_{sw}$ ; (g) the trench-normal component of the subduction velocity  $v_{sn}$ ; (h) the trench-normal component of the convergence velocity  $v_{cn}$ ; and (i) the long wavelength (i.e., 80–100 km) roughness  $R_{lw}$ . Each dot represents one of the 62 subduction zone segments. Correlation coefficients and  $p$ -values are indicated for both the Spearman and Pearson methods. The names of the subduction zone segments are indicated for isolated points in the scatter plots. The threshold of 0.2 for the multivariate analysis is indicated by the blue rectangle. Abbreviations for parameters are explained in Tables 1 and 2.

299 with class 1 containing subduction zone segments with few tsunamigenic earthquakes (i.e.,  $N_t < 0.2$ ), and class 2 containing subduction zone segments with a large number of tsunamigenic earthquakes (i.e.,  $N_t \geq 0.2$ ). The threshold  
 300 of 0.2 is chosen because it seems to naturally divide the data in the case of the bivariate analysis, as shown in the scatter  
 301 plots of the age, sediment thickness, and type of margin in Fig. 5. Using different thresholds ranging from 0–0.3  
 302 slightly changes the parameters that are most effective in dividing the two classes, but in general the combination of  
 303 parameters is consistent.

304  
 305 The Fisher discriminant analysis typically consists of a learning phase, a voting phase, and control experiments  
 306 (e.g., Sandri et al., 2004, and references therein). However, following Brizzi et al. (2018), we confine our analysis to  
 307 the learning phase due to the limited amount of data. During the learning phase, an input set of  $n$  parameters is  
 308 used to identify all the possible linear combinations consisting of  $k = 1, \dots, n$  parameters. To distinguish the effect of  
 309 multiple parameters that could be interdependent, we run 36 Fisher analyses to systematically test the effect of the  
 310 parameters. The parameters  $A$ ,  $D_{arc-trench}$ , and  $UPS$  are independent parameters that are always included in the  
 311 analysis.  $T_{sed}$  and  $AvsE$  (i.e., the type of margin: accretionary or erosional) are dependent on each other as larger

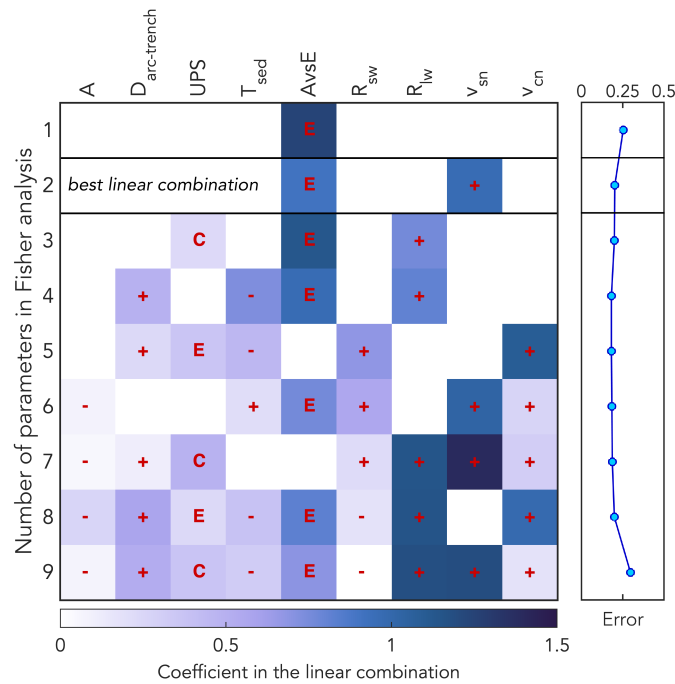


**Figure 6** Representative Fisher analysis for one set of input parameters (listed at the top). When a parameter is included in the linear combination, a red symbol indicates how it promotes class 2 ( $N_t \geq 0.2$ ). Hence, a plus indicates that larger values of a parameter are associated with class 2. For discrete parameters, letters indicate the most favourable setting for class 2 (Table 1). The right panel shows the error reduction when more parameters are included in the linear combination. The optimal linear combination for which the error is maximally reduced for the least amount of features included in the linear combination is indicated by black lines.

sediment thickness is usually associated with accretionary margins, whereas small sediment thickness is typically associated with erosional margins. Therefore, we run three different test cases: one in which both parameters are included and two where each parameter is included separately. The same reasoning holds for the two measures of incoming plate roughness  $R_{sw}$  and  $R_{lw}$ . We adopt a similar reasoning for the velocities  $v_{sn}$ ,  $v_{cn}$ , but we also include the option to exclude both velocities from the linear combination, because they could potentially relate to the limited time span of observations in addition to a physical mechanism. This then results in a total of  $3 \cdot 3 \cdot 4 = 36$  different sets of input parameters for the Fisher analysis. For a given set of input parameters, there is one linear combination with a minimum number of parameters  $k_m$  that minimises the error: the optimal linear combination (Fig. 6). For each analysis, we automatically detect this optimal linear combination when the error reduction by including more parameters into the analysis becomes less than 5% with respect to the initial error in the case of including only one parameter. Hence, we end up with an optimal linear combination for each of the 36 Fisher analyses. The coefficients in the linear combinations indicate the importance of a parameter in the combination.

To systematically determine which parameters are the most important for generating tsunamigenic earthquakes, we look at three measures: (i) the fraction that a parameter is picked in the best linear combination for a Fisher analysis when it is part of the input; (ii) the normalised average coefficient of a parameter based on all Fisher analyses for which it is included in the best linear combination; (iii) the maximum fraction of a consistent sign (i.e., positive or negative) of the coefficient of a parameter to account for the robustness of the effect of the parameter in the linear combination. We define the measure of relative importance  $RI$  of a parameter as the multiplication of these three measures.

## 4.2 Results

Fig. 6 shows the results for one representative Fisher analysis. The input parameters used in the test are indicated at the top, and the resulting coefficients of the linear combinations for different numbers of parameters allowed in the linear combination (on the  $y$ -axis) is indicated by the colours in each row. Parameters are part of the linear combination when a red symbol is present in the relevant square.

If only one parameter is used to distinguish the two classes of few (class 1;  $N_t < 0.2$ ) and many (class 2;  $N_t \geq 0.2$ ) tsunamigenic earthquakes, the type of margin  $AvsE$  is the deciding factor. In this case, an erosional margin is more favourable to produce many tsunamis. When a second parameter is allowed to enter the linear combination that divides the two classes, the trench-normal component of the subduction velocity is picked by the Fisher algorithm. The positive coefficient indicates that a large subduction velocity correlates to class 2, i.e., many tsunamigenic earthquakes. These two parameters,  $AvsE$  and  $v_{sn}$ , also exhibited high correlations in the bivariate analysis (Sec. 3.2.4). The combination of these two parameters is also the optimal linear combination as defined in Sec. 4.1. The error is

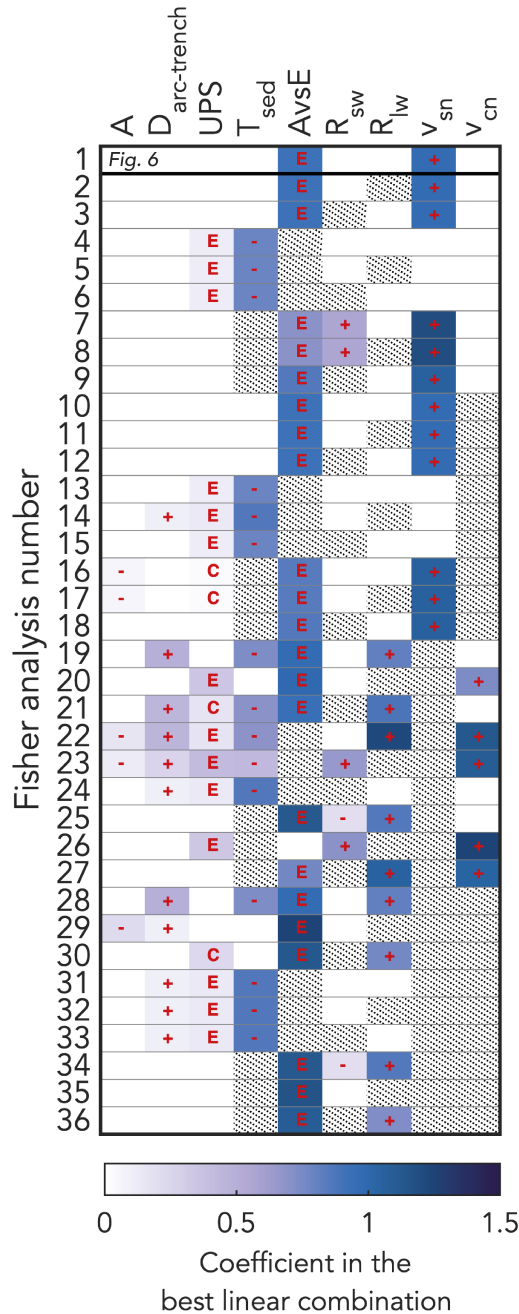


**Figure 7** The best linear combination for each Fisher analysis. When a parameter is included in the linear combination, a red symbol indicates how it promotes class 2 ( $N_t \geq 0.2$ ). Hence, a plus indicates that larger values of a parameter are associated with class 2. For discrete parameters, letters indicate the most favourable setting for class 2 (Table 1). If parameters are not included in the input for a test, the area is dotted. Note that the best linear combination of Fig. 6 is included here as well and highlighted by horizontal black lines.

namely reduced the most with respect to the least amount of features required to divide the two classes. When a third parameter enters the linear combination, the upper plate strain  $UPS$  is picked by the Fisher analysis. An overriding plate that experiences compression is associated with many tsunamis. Simultaneously, the long wavelength roughness  $R_{lw}$  is picked instead of the subduction velocity, indicating that a rougher incoming plate is associated with the class of many tsunamis. With four parameters, the upper plate strain is removed from the linear combination, and instead the sediment thickness  $T_{sed}$  and the distance between the volcanic arc and the trench  $D_{arc-trench}$  are picked. As  $D_{arc-trench}$  can be related to the dip of a slab, with large  $D_{arc-trench}$  being associated with a more shallowly dipping slab, a positive coefficient in the linear combination could hint at a relationship between shallowly dipping slabs and tsunamigenic earthquakes. The negative coefficient of the sediment thickness  $T_{sed}$  associated here with many tsunamis is in line with the erosional margin that is consistently present in almost all linear combinations.

When all 9 parameters are included in the linear combination, which is theoretically possible, the error is higher compared to the best linear combination. This indicates that including more parameters into the linear combina-

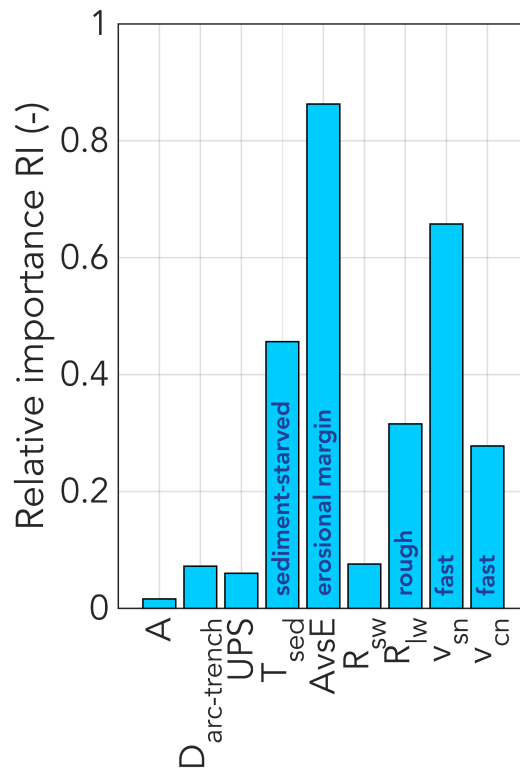


**Figure 8** The relative importance of parameters (Sec. 4.1) as calculated from the Fisher analyses presented in Fig. 7. For parameters with a relative importance  $RI > 0.2$ , text in the bars indicates how the parameter promotes many tsunamigenic earthquakes (class 2).

tion does not necessarily improve it. Also note that the parameters chosen for the linear combinations can differ completely when a different number of parameters is allowed for the linear combination. The sign of the parameter can also change for different numbers of parameters. When the sign consistently remains the same over all linear combinations and Fisher analyses, we deem the effect of the parameter on dividing the two classes to be robust. In summary, for the example Fisher analysis of Fig. 6, the linear combination that best describes the difference between the two classes with these parameters as input consists of the type of margin and the subduction velocity.

When we consider all 36 Fisher analyses, the amount of parameters included in the best linear combination is on average 2.9. The maximum amount of parameters included in the optimal linear combination is 6. The error associated with the best linear combination is on average 0.22. This corresponds to an average of 10.5 segments (16.9%) that are classified in the wrong class according to the optimal linear combination. The best linear combinations for each of the 36 Fisher analyses that were run for different combinations of input parameters are shown in Fig. 7. Several variables appear to stand out, such as the type of margin (consistently erosional) and the subduction velocity (consistently positive). We summarise the main findings of these 36 analyses in Fig. 8, by calculating the relative importance of each parameter as described in Sec. 4.1.

The most important parameter, with a relative importance of 0.86, is the type of margin, i.e., accretionary or erosional. When it is included in the input parameters of the Fisher analysis, it is picked 95.8% of the time in the best linear combination. After that, the second most important parameter is the trench-normal component of the subduction velocity with relative importance 0.66, which is picked 66.7% of the time. The third most important parameter is the sediment thickness with  $RI = 0.46$ , which is picked 50% of the time. The long wavelength roughness has a relative importance of 0.32 and the trench-normal component of the convergence velocity has  $RI = 0.28$ . The other parameters show low measures of relative importance with  $RI < 0.1$ . Hence, based on these results, subduction zones are more prone to host tsunamigenic earthquakes at an erosional margin with few sediments and a rough incoming seafloor in a rapidly converging system.

## 5 Discussion

We compiled the SNITCH database consisting of tsunami characteristics, tsunamigenic earthquake parameters, megathrust seismicity, seismogenic zone geometry, and tectonic parameters of subduction zones across the world. Due to the constraints on the tsunami data availability, we focus the interpretation of the results on the normalised number of tsunamis per subduction zone segment  $N_t$ , as this is a measure that is available for every segment. This ensures that the results we present and the analyses that we do are statistically significant. Generally the amount of tsunamigenesis depends on the amount of large earthquakes that has occurred in a subduction zone. This is captured in our

analysis, as we find significant correlations in the bivariate analysis (Sec. 3) between  $N_t$  and various measures of the maximum earthquake magnitude a subduction zone segment has experienced. This indicates the robustness of  $N_t$  as a useful measure for tsunamigenic potential in subduction zones.

The bivariate analysis further shows that the normalised number of tsunamis per km trench  $N_t$  correlates with some of the interplate seismicity and tectonic parameters in SNITCH-SN. However,  $N_t$  shows no correlation with the geometric parameters describing the seismogenic zone. Specifically, meaningful correlations are found with the type of margin (i.e., accretionary or erosional), the trench-normal components of the subduction and convergence velocity of the subduction zone, the sediment thickness, seismicity rate, and measures of maximum earthquake magnitude in a subduction zone segment.

The multivariate analysis of the tectonic parameters points towards the same parameters identified in the bivariate analysis and to the incoming plate roughness, to distinguish subduction zones with a lower ( $N_t < 0.2$ ) and higher number of tsunamigenic earthquakes ( $N_t \geq 0.2$ ). Specifically, we find that rough incoming plates at erosional margins, in rapidly converging systems have produced more tsunamigenic earthquakes during the analysed time span.

In the following, we discuss which - if any - tectonic setting is more favourable for tsunamigenic earthquakes and how this could affect tsunamigenesis. We also speculate which kind of fault is likely to be the most important in producing tsunamigenic earthquakes, because we did not find a correlation with the seismogenic zone geometry parameters.

## 5.1 Are there specific tectonic settings where more tsunamigenic earthquakes have been observed?

We find multiple significant correlations and patterns in both the bivariate and multivariate analyses, indicating that certain parameters are indeed correlated with an increased amount of observed tsunamis. So, we show that there are indeed specific tectonic settings where more tsunamigenic earthquakes have been observed. Therefore, we speculate that there are specific tectonic settings that could be more prone to host tsunamigenic earthquakes (Sec. 5.2). However, most scatter plots still contain outliers (Fig. 5) and there are always at least 8 segments (12.9%) incorrectly classified in the multivariate analysis (Sec. 4.2). Besides that, for some parameters no clear correlation can be discerned at all. This is partly due to the limited amount of data for the 62 subduction zone segments. Most parameters in the SNITCH database do not have values for each subduction zone segment due to a lack of observations.

In addition, we only consider a limited observational time span for the data in this study, with the earthquake data limited to 1900–2007 and the tsunami data limited to 1962–2018 (or, for comparison to the earthquake parameters, 2007). The time span is constrained by the availability of as-complete-as-possible global coverage of tsunami and earthquake observations. Incorporating data from outside this observational time window would skew the results of our statistical analysis by adding a bias towards large (that is, easily observable) earthquakes and tsunamis. Hence, as a result of the limited observational time window SNITCH-T does not include large historical tsunamigenic earthquakes such as the 1944  $M_w$  8.0–8.3 Tonankai, 1946  $M_w$  8.1–8.4 Nankaido (Kanamori, 1972b), and 1960  $M_w$  9.4–9.6 Chile (Kanamori and Cipar, 1974; Satake and Atwater, 2007) earthquakes. Therefore, the tsunamigenic potential of these regions might be underestimated in our analysis.

Interestingly, the seismogenic zone geometry parameters (Sec. 3.2.3) do not correlate with  $N_t$ , which can have different explanations. First, it might be that the amount of data present in our tsunami databases is too scarce to result in any significant correlation (Fig. 3). However, other parameters do show significant correlations, so this option is not necessarily true. An alternative explanation might be that the megathrust is not the most important fault in tsunamigenesis. Because of that, the seismogenic zone parameters that define the potential slip area on the megathrust do not correlate with  $N_t$ . We explore this option in more detail in Sec. 5.3.

## 5.2 Which tectonic setting is more prone to host tsunamigenic earthquakes?

Our analysis shows that subduction zones where the incoming plate subducts rapidly at an erosional margin are likely more prone to generate tsunamis through earthquakes (Fig. 9). Our analysis also highlights the importance of having a thin sediment layer in the subduction segment in order to be associated with more tsunamigenic earthquakes. The effect of a thin sediment layer on tsunamigenic earthquake occurrence in subduction zones fits well with the importance of erosional margins, because sediment-starved trenches are often associated with erosional margins. However, this does not mean that erosional margins are completely devoid of sediment cover (Clift and Vannucchi, 2004). It has been suggested that the presence of sediments could enhance tsunamigenesis, by promoting larger uplift (Ma and Nie, 2019). This could explain the large range of  $N_t$  for subduction zone segments with moderate sediment cover (i.e.,  $T_{\text{sed}} \leq 2$  km; Fig. 5d). Therefore, erosional margins with a small sedimentary wedge may be more prone to host tsunamigenic earthquakes. The negative correlation between sediment thickness and the amount of normalised tsunamis in a subduction zone segment could also be related to the effect of sediment thickness on the recurrence time of earthquakes. For example, the modelling study of Brizzi et al. (2020) shows that less sediment cover results in a smaller seismogenic zone with a shorter recurrence interval. Here, we find that subduction zone segments with a thick sedimentary layer — and, presumably, a larger recurrence interval — have produced less tsunamis,

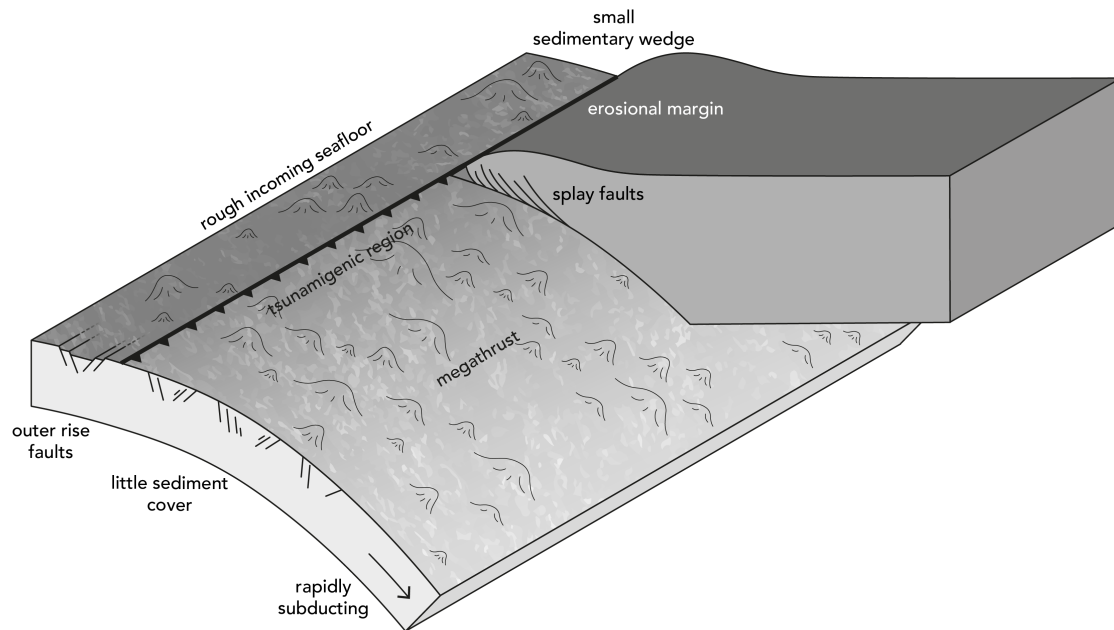


**Figure 9** Cartoon of a tectonic setting more prone to host tsunamigenic earthquakes. A subducting slab with little sediments and a rough incoming seafloor subducts relatively rapidly beneath a continental plate at an erosional margin.

443 which could be a result of the limited observational time span of the SNITCH database (Sec. 5.1). One outlier that is  
 444 apparent in Fig. 5e is the Nankai subduction segment, which has produced relatively many tsunamis even though it  
 445 is an accretionary margin rather than erosional. However, the Nankai segment has experienced periods of erosion  
 446 (Clift and Vannucchi, 2004), which might explain why it has experienced more tsunamis than the other accretionary  
 447 margins. The Nankai subduction segment is also characterised by a rough subducting plate with many topographical  
 448 features such as seamounts (Yokota et al., 2016). Since we find that rough subducting plates are associated with more  
 449 tsunamigenic earthquakes, this could also contribute towards the reason as to why Nankai is an outlier.

450 The importance of the trench-normal components of the subduction and convergence velocity can be explained  
 451 through the general relationship between earthquakes and tsunamis also found in the bivariate analysis (Sec. 3.2;  
 452 Fig. 3). In a subduction zone with a high subduction or convergence velocity, the stresses are built up faster and  
 453 hence released more often in earthquakes, resulting in a shorter recurrence interval. More earthquakes generally  
 454 means a larger likelihood of those earthquakes producing tsunamis. Since our study is restricted to a specific time  
 455 interval for tsunamigenic earthquake observations, it is indeed likely that the subduction zones with a higher con-  
 456 vergence velocity have produced more tsunamigenic earthquakes in this time period (McCaffrey, 2008; Corbi et al.,  
 457 2017). An alternative explanation for the importance of the velocities could be that large convergence velocities are  
 458 typically associated with erosional margins (Clift and Vannucchi, 2004). Since we find that erosional margins are the  
 459 most important factor for increased tsunamigenesis, it follows that the two aspects associated most with erosional  
 460 margins, i.e., fast convergence and a thin sediment cover, are also highlighted in our analysis as important factors  
 461 for tsunamigenesis.

462 Other studies have already linked sediment thickness at the trench and seafloor roughness to tsunami earthquakes  
 463 (Tanioka et al., 1997; Polet and Kanamori, 2000; Wang and Lin, 2022). The combination of a thin sediment layer at the  
 464 trench and a rough seafloor in particular has already been pointed out for 13 tsunami earthquake regions at 7 different  
 465 subduction zones (i.e., Sumatra, Java, Hokkaido and the Kurils, Aleutians, Nicaragua, Peru, and New Zealand) by  
 466 Geersen (2019). They looked at structural similarities between marine acoustic data. Our study strengthens this view  
 467 by providing the first global, statistical analysis of the effect of these parameters on tsunamigenic earthquakes, which  
 468 include both tsunami earthquakes and large megathrust earthquakes that caused tsunamis. The amount of trench  
 469 sediments and the roughness of the seafloor are often considered as related, because thick piles of sediment entering  
 470 the trench could potentially smooth out the topography on the incoming plate (Ruff, 1989). It is generally thought that  
 471 a rough incoming seafloor and lack of sediments leads to a complex, heavily fractured shallow subduction interface  
 472 (Dominguez et al., 1998; Wang and Bilek, 2011, 2014; Ruh et al., 2016). Such a heavily fractured environment could  
 473 promote tsunamigenic earthquakes, because of the increased presence of splay faults that can accommodate large  
 474 vertical displacement.



### 5.3 Which type of fault produces tsunamigenic earthquakes?

Large tsunamis have been caused by large earthquakes that ruptured the megathrust, such as the 2004  $M_w$  9.1–9.3 Sumatra-Andaman (e.g., Lay et al., 2005; Titov et al., 2005), 2010  $M_w$  8.8 Maule (e.g., Delouis et al., 2010), and 2011  $M_w$  9.0 Tōhoku-Oki earthquake (e.g., Fujii et al., 2011; Ozawa et al., 2011). They have also been caused by smaller earthquakes that potentially ruptured outer rise or splay faults, such as the 1933  $M_w$  8.4 Sanriku (Kanamori, 1971), 1946 Unimak Alaska (von Huene et al., 2016), and 2006 Java (Fan et al., 2017) tsunami earthquakes. Simultaneously, splay faults could also play a role during large megathrust earthquakes, as suggested for the 2004  $M_w$  9.1–9.3 Sumatra-Andaman (DeDontney and Rice, 2012; Waldhauser et al., 2012) and the 2010  $M_w$  8.8 Maule (Melnick et al., 2012) earthquakes.

Our study shows a lack of correlations between  $N_t$  and the seismogenic zone geometry parameters, as discussed in Sec. 5.1. This could result from the fact that the megathrust is not the most important fault to produce tsunamigenic earthquakes. Indeed, many studies have proposed that outer rise or splay faults play an important role for tsunamigenesis (e.g., Fukao, 1979; Wendt et al., 2009; Sladen and Trevisan, 2018; Van Zelst et al., 2022). Slip on these types of faults, which are typically steeper than the megathrust, could result in larger vertical displacement compared to megathrust events. This could explain the discrepancy between earthquake moment magnitude and tsunami magnitude observed during tsunami earthquakes (Kanamori, 1972a). It could also explain why we find that erosional margins have produced more tsunamigenic earthquakes, since they are typically associated with a heavily fractured environment including splay faults. Hence, we speculate that faults other than the megathrust might play an equally, or more, important role in tsunamigenesis.

## 6 Conclusions

We compiled the SNITCH database, which contains global data on earthquake and tectonic subduction zone features, tsunamis, and tsunamigenic earthquakes for 62 subduction segments. In the performed bivariate analysis, we find correlations between the normalised number of tsunamigenic earthquakes per km trench  $N_t$  of the SNITCH-T database and some of the tectonic parameters of the SNITCH-SN database (i.e., the type of margin: accretionary or erosional, the trench-normal components of the subduction and convergence velocity, and the sediment thickness at the trench).

The multivariate analysis explores the relationships between the tectonic parameters and the tsunamigenic potential of a subduction zone further. The type of margin (i.e., erosional or accretionary) and the subduction and convergence velocity normal to the trench are the most crucial parameters to sort the subduction zones between a class with few tsunamigenic earthquakes ( $N_t < 0.2$ ) and a class with many tsunamigenic earthquakes ( $N_t \geq 0.2$ ). Other parameters of secondary importance for this division are the long wavelength roughness and the sediment thickness at the trench. Tsunamigenic earthquakes therefore appear to be more common in rapidly converging, erosional subduction settings, with a rough incoming plate and low amounts of sediments at the trench. These settings are characterised by heavily fractured and complex, heterogeneous shallow subduction interfaces arising from the rough seafloor and the lack of sediments smoothing the interface. Tsunamigenic earthquakes may be more common in such settings, because of the presence of more splay faults, which could accommodate larger vertical displacements.

## Acknowledgements

We would like to thank Andreas Fichtner for fruitful discussions and support that greatly improved this work. We are also grateful to Arnauld Heuret, Claudia Piromallo, and Serge Lallemand, for providing and helping with the SNITCH-SN database. We thank Laura Sandri for helping with setting up the Fisher analysis.

This work is part of the ASCETE project funded by the Volkswagen Foundation (Advanced Simulation of Coupled Earthquake-Tsunami Events, grant no 88479). The grant to the Department of Science, Roma Tre University (MIUR-Italy Dipartimenti di Eccellenza, articolo 1, commi 314 – 337, legge 232/2016) is gratefully acknowledged by FF, SB and EvR. IvZ acknowledges the financial support and endorsement from the DLR Management Board Young Research Group Leader Program and the Executive Board Member for Space Research and Technology.

Throughout this work, we use scientific colour maps by Crameri (2018) to prevent visual distortion of the data and exclusion of readers with colour-vision deficiencies (Crameri et al., 2020).

## Data and code availability

The SNITCH database, coordinates of the subduction zone segments, and MATLAB scripts to reproduce this study can be found in Van Zelst (2022). (*note: the files are uploaded to Zenodo and the DOI is reserved, but they are not officially published yet since there may still be changes to the scripts before acceptance. Because of that, the doi link does not work yet. The Zenodo repository is therefore included as an attachment to this article submission as an interim solution.*)

## 528 Competing interests

529 The authors have no competing interests.

## 530 References

- 531 Bell, R., Holden, C., Power, W., Wang, X., and Downes, G. Hikurangi margin tsunami earthquake generated by slow seismic rupture over a  
532 subducted seamount. *Earth and Planetary Science Letters*, 397:1–9, 2014. doi: <https://doi.org/10.1016/j.epsl.2014.04.005>.
- 533 Bilek, S. L. The role of subduction erosion on seismicity. *Geology*, 38(5):479–480, 2010. doi: <https://doi.org/10.1130/focus052010.1>.
- 534 Bilek, S. L. and Lay, T. Rigidity variations with depth along interplate megathrust faults in subduction zones. *Nature*, 400(6743):443, 1999.  
535 doi: <https://doi.org/10.1038/22739>.
- 536 Bilek, S. L. and Lay, T. Tsunami earthquakes possibly widespread manifestations of frictional conditional stability. *Geophysical Research  
537 Letters*, 29(14):18–1, 2002. doi: <https://doi.org/10.1029/2002GL015215>.
- 538 Brizzi, S., Sandri, L., Funicello, F., Corbi, F., Piromallo, C., and Heuret, A. Multivariate statistical analysis to investigate the subduc-  
539 tion zone parameters favoring the occurrence of giant megathrust earthquakes. *Tectonophysics*, 728:92–103, 2018. doi: <https://doi.org/10.1016/j.tecto.2018.01.027>.
- 541 Brizzi, S., Van Zelst, I., Funicello, F., Corbi, F., and van Dinther, Y. How sediment thickness influences subduction dynamics and seismicity.  
542 *Journal of Geophysical Research: Solid Earth*, 125(8):e2019JB018964, 2020. doi: <https://doi.org/10.1029/2019JB018964>.
- 543 Carvajal, M., Sun, T., Wang, K., Luo, H., and Zhu, Y. Evaluating the tsunamigenic potential of buried versus trench-breaching megathrust  
544 slip. *Journal of Geophysical Research: Solid Earth*, 127(8):e2021JB023722, 2022. doi: <https://doi.org/10.1029/2021JB023722>.
- 545 Clift, P. and Vannucchi, P. Controls on tectonic accretion versus erosion in subduction zones: Implications for the origin and recycling of  
546 the continental crust. *Reviews of Geophysics*, 42(2), 2004. doi: <https://doi.org/10.1029/2003RG000127>.
- 547 Corbi, F., Funicello, F., Brizzi, S., Lallemand, S., and Rosenau, M. Control of asperities size and spacing on seismic behavior of subduction  
548 megathrusts. *Geophysical Research Letters*, 44, 2017. doi: <https://doi.org/10.1002/2017GL074182>.
- 549 Cramer, F. Scientific colour-maps, 2018.
- 550 Cramer, F., Shephard, G. E., and Heron, P. J. The misuse of colour in science communication. *Nature communications*, 11(1):1–10, 2020.
- 551 DeDontney, N. and Rice, J. R. Tsunami wave analysis and possibility of splay fault rupture during the 2004 Indian Ocean earthquake. *Pure  
552 and applied geophysics*, 169(10):1707–1735, 2012. doi: <https://doi.org/10.1007/s00024-011-0438-4>.
- 553 Delouis, B., Nocquet, J.-M., and Vallée, M. Slip distribution of the February 27, 2010 Mw= 8.8 Maule earthquake, central Chile,  
554 from static and high-rate GPS, InSAR, and broadband teleseismic data. *Geophysical Research Letters*, 37(17), 2010. doi: <https://doi.org/10.1029/2010GL043899>.
- 556 DeMets, C., Gordon, R. G., Argus, D., and Stein, S. Current plate motions. *Geophysical journal international*, 101(2):425–478, 1990.  
557 doi: <https://doi.org/10.1111/j.1365-246X.1990.tb06579.x>.
- 558 Dominguez, S., Lallemand, S., Malavieille, J., and von Huene, R. Upper plate deformation associated with seamount subduction. *Tectono-  
559 physics*, 293(3-4):207–224, 1998. doi: [https://doi.org/10.1016/S0040-1951\(98\)00086-9](https://doi.org/10.1016/S0040-1951(98)00086-9).
- 560 Duda, R. O., Hart, P. E., and Stork, D. G. *Pattern classification and scene analysis*, volume 3. Wiley New York, 1973.
- 561 Fan, W., Bassett, D., Jiang, J., Shearer, P. M., and Ji, C. Rupture evolution of the 2006 Java tsunami earthquake and the possible role of splay  
562 faults. *Tectonophysics*, 721:143–150, 2017. doi: <https://doi.org/10.1016/j.tecto.2017.10.003>.
- 563 Faulkner, D., Mitchell, T., Behn, S., Hirose, T., and Shimamoto, T. Stuck in the mud? Earthquake nucleation and propagation through  
564 accretionary forearcs. *Geophysical Research Letters*, 38(18), 2011. doi: <https://doi.org/10.1029/2011GL048552>.
- 565 Fujii, Y., Satake, K., Sakai, S., Shinohara, M., and Kanazawa, T. Tsunami source of the 2011 off the Pacific coast of Tohoku Earthquake. *Earth,  
566 planets and space*, 63(7):55, 2011. doi: <https://doi.org/10.5047/eps.2011.06.010>.
- 567 Fukao, Y. Tsunami earthquakes and subduction processes near deep-sea trenches. *Journal of Geophysical Research: Solid Earth*, 84(B5):  
568 2303–2314, 1979. doi: <https://doi.org/10.1029/JB084iB05p02303>.
- 569 Gahalaut, V., Subrahmanyam, C., Kundu, B., Catherine, J., and Ambikapathy, A. Slow rupture in Andaman during 2004 Sumatra-  
570 Andaman earthquake: a probable consequence of subduction of 90E ridge. *Geophysical Journal International*, 180(3):1181–1186, 2010.  
571 doi: <https://doi.org/10.1111/j.1365-246X.2009.04449.x>.
- 572 Geersen, J. Sediment-starved trenches and rough subducting plates are conducive to tsunami earthquakes. *Tectonophysics*, 762:28–44,  
573 2019. doi: <https://doi.org/10.1016/j.tecto.2019.04.024>.
- 574 Global Historical Tsunami Database. National Geophysical Data Center / World Data Service (NGDC/WDS), Retrieved: February 1, 2019.  
575 <https://doi.org/10.7289/V5PN93H7>.
- 576 Gusiakov, V. K., Dunbar, P. K., and Arcos, N. Twenty-five years (1992–2016) of global tsunamis: Statistical and analytical overview. *Pure and  
577 Applied Geophysics*, pages 1–13, 2019. doi: <https://doi.org/10.1007/s00024-019-02113-7>.
- 578 Heuret, A., Lallemand, S., Funicello, F., Piromallo, C., and Faccenna, C. Physical characteristics of subduction interface type seismogenic  
579 zones revisited. *Geochemistry, Geophysics, Geosystems*, 12(1), 2011. doi: <https://doi.org/10.1029/2010GC003230>.
- 580 Heuret, A., Conrad, C., Funicello, F., Lallemand, S., and Sandri, L. Relation between subduction megathrust earthquakes, trench sediment  
581 thickness and upper plate strain. *Geophysical Research Letters*, 39(5), 2012. doi: <https://doi.org/10.1029/2011GL050712>.
- 582 Iida, K., Cox, D. C., and Paras-Carayannis, G. Preliminary catalog of tsunamis occurring in the Pacific Ocean. Technical report, DTIC  
583 Document, 1967.

- 584 Jiang, Y., González, P. J., and Bürgmann, R. Subduction earthquakes controlled by incoming plate geometry: The 2020  $m > 7.5$  Shumagin,  
585 Alaska, earthquake doublet. *Earth and Planetary Science Letters*, 584:117447, 2022. doi: <https://doi.org/10.1016/j.epsl.2022.117447>.
- 586 Kanamori, H. Seismological evidence for a lithospheric normal faulting – The Sanriku earthquake of 1933. *Physics of the Earth and Planetary  
587 Interiors*, 4(4):289–300, 1971. doi: [https://doi.org/10.1016/0031-9201\(71\)90013-6](https://doi.org/10.1016/0031-9201(71)90013-6).
- 588 Kanamori, H. Mechanism of tsunami earthquakes. *Physics of the earth and planetary interiors*, 6(5):346–359, 1972a. doi: [https://doi.org/10.1016/0031-9201\(72\)90058-1](https://doi.org/10.1016/0031-9201(72)90058-1).
- 590 Kanamori, H. Tectonic implications of the 1944 Tonankai and the 1946 Nankaido earthquakes. *Physics of the Earth and Planetary Interiors*,  
591 5:129–139, 1972b. doi: [https://doi.org/10.1016/0031-9201\(72\)90082-9](https://doi.org/10.1016/0031-9201(72)90082-9).
- 592 Kanamori, H. and Cipar, J. J. Focal process of the great Chilean earthquake May 22, 1960. *Physics of the Earth and Planetary Interiors*, 9(2):  
593 128–136, 1974.
- 594 Lallemand, S., Peyret, M., Van Rijsingen, E., Arcay, D., and Heuret, A. Roughness characteristics of oceanic seafloor prior to subduction in  
595 relation to the seismogenic potential of subduction zones. *Geochemistry, Geophysics, Geosystems*, 19(7):2121–2146, 2018. doi: <https://doi.org/10.1029/2018GC007434>.
- 597 Lay, T., Kanamori, H., Ammon, C. J., Nettles, M., Ward, S. N., Aster, R. C., Beck, S. L., Bilek, S. L., Brudzinski, M. R., Butler, R.,  
598 et al. The great Sumatra-Andaman earthquake of 26 December 2004. *Science*, 308(5725):1127–1133, 2005. doi: <https://doi.org/10.1126/science.1112250>.
- 600 Lay, T., Kanamori, H., Ammon, C. J., Koper, K. D., Hutko, A. R., Ye, L., Yue, H., and Rushing, T. M. Depth-varying rupture properties of subduc-  
601 tion zone megathrust faults. *Journal of Geophysical Research: Solid Earth*, 117(B4), 2012. doi: <https://doi.org/10.1029/2011JB009133>.
- 602 López, A. M. and Okal, E. A. A seismological reassessment of the source of the 1946 Aleutian ‘tsunami’ earthquake. *Geophysical Journal  
603 International*, 165(3):835–849, 2006. doi: <https://doi.org/10.1111/j.1365-246X.2006.02899.x>.
- 604 Ma, S. and Nie, S. Dynamic Wedge Failure and Along-Arc Variations of Tsunamigenesis in the Japan Trench Margin. *Geophysical Research  
605 Letters*, 2019. doi: <https://doi.org/10.1029/2019GL083148>.
- 606 McCaffrey, R. Global frequency of magnitude 9 earthquakes. *Geology*, 36(3):263–266, 2008. doi: <https://doi.org/10.1130/G24402A.1>.
- 607 Melnick, D., Moreno, M., Motagh, M., Cisternas, M., and Wesson, R. L. Splay fault slip during the Mw 8.8 2010 Maule Chile earthquake.  
608 *Geology*, 40(3):251–254, 2012. doi: <https://doi.org/10.1130/G32712.1>.
- 609 Oryan, B. and Buck, W. R. Larger tsunamis from megathrust earthquakes where slab dip is reduced. *Nature Geoscience*, 13(4):319–324,  
610 2020. doi: <https://doi.org/10.1038/s41561-020-0553-x>.
- 611 Ozawa, S., Nishimura, T., Suito, H., Kobayashi, T., Tobita, M., and Imakiire, T. Coseismic and postseismic slip of the 2011 magnitude-9  
612 Tohoku-Oki earthquake. *Nature*, 475(7356):373, 2011. doi: <https://doi.org/10.1038/nature10227>.
- 613 Polet, J. and Kanamori, H. Shallow subduction zone earthquakes and their tsunamigenic potential. *Geophysical Journal International*, 142  
614 (3):684–702, 2000. doi: <https://doi.org/10.1046/j.1365-246x.2000.00205.x>.
- 615 Robinson, D., Das, S., and Watts, A. Earthquake rupture stalled by a subducting fracture zone. *Science*, 312(5777):1203–1205, 2006.  
616 doi: <https://doi.org/10.1126/science.1125771>.
- 617 Ruff, L. and Kanamori, H. Seismicity and the subduction process. *Physics of the Earth and Planetary Interiors*, 23(3):240–252, 1980.  
618 doi: [https://doi.org/10.1016/0031-9201\(80\)90117-X](https://doi.org/10.1016/0031-9201(80)90117-X).
- 619 Ruff, L. J. Do trench sediments affect great earthquake occurrence in subduction zones? In *Subduction Zones Part II*, pages 263–282.  
620 Springer, 1989. doi: <https://doi.org/10.1007/BF00874629>.
- 621 Ruh, J. B., Sallarès, V., Ranero, C. R., and Gerya, T. Crustal deformation dynamics and stress evolution during seamount subduc-  
622 tion: High-resolution 3-d numerical modeling. *Journal of Geophysical Research: Solid Earth*, 121(9):6880–6902, 2016. doi: <https://doi.org/10.1002/2016JB013250>.
- 624 Sahakian, V., Melgar, D., and Muzli, M. Weak near-field behavior of a tsunami earthquake: Towards real-time identification for local warning.  
625 *Geophysical Research Letters*, 2019. doi: <https://doi.org/10.1029/2019GL083989>.
- 626 Sandri, L., Marzocchi, W., and Zaccarelli, L. A new perspective in identifying the precursory patterns of eruptions. *Bulletin of volcanology*,  
627 66(3):263–275, 2004. doi: <https://doi.org/10.1007/s00445-003-0309-7>.
- 628 Satake, K. 4.19 - Tsunamis. In Schubert, G., editor, *Treatise on Geophysics*, pages 477 – 504. Elsevier, Oxford, second edition, 2015.  
629 doi: <https://doi.org/10.1016/B978-0-444-53802-4.00086-5>.
- 630 Satake, K. and Atwater, B. F. Long-term perspectives on giant earthquakes and tsunamis at subduction zones. *Annu. Rev. Earth Planet. Sci.*,  
631 35:349–374, 2007.
- 632 Satake, K. and Tanioka, Y. Sources of tsunami and tsunamigenic earthquakes in subduction zones. *Pure and Applied Geophysics*, 154(3-4):  
633 467–483, 1999. doi: <https://doi.org/10.1007/s000240050240>.
- 634 Scholl, D. W., Kirby, S. H., von Huene, R., Ryan, H., Wells, R. E., and Geist, E. L. Great ( $\geq$  Mw8.0) megathrust earthquakes and the subduction  
635 of excess sediment and bathymetrically smooth seafloor. *Geosphere*, 11(2):236–265, 2015. doi: <https://doi.org/10.1130/GES01079.1>.
- 636 Seno, T. Tsunami earthquakes as transient phenomena. *Geophysical research letters*, 29(10), 2002. doi: <https://doi.org/10.1029/2002GL014868>.
- 638 Sibuet, J.-C., Rangin, C., Le Pichon, X., Singh, S., Cattaneo, A., Graindorge, D., Klingelhoefer, F., Lin, J.-Y., Malod, J., Maury, T., et al. 26th  
639 December 2004 great Sumatra-Andaman earthquake: Co-seismic and post-seismic motions in northern Sumatra. *Earth and Planetary  
640 Science Letters*, 263(1-2):88–103, 2007. doi: <https://doi.org/10.1016/j.epsl.2007.09.005>.
- 641 Sladen, A. and Trevisan, J. Shallow megathrust earthquake ruptures betrayed by their outer-trench aftershocks signature. *Earth and  
642 Planetary Science Letters*, 483:105–113, 2018. doi: <https://doi.org/10.1016/j.epsl.2017.12.006>.
- 643 Soloviev, S. and Go, C. N. Catalog of tsunamis in western coast of the Pacific Ocean. *Academy of Sciences, USSR, Izdat. Nauka*, pages 1–130,

- 1974.
- 645 Storchak, D. A., Di Giacomo, D., Bondár, I., Engdahl, E. R., Harris, J., Lee, W. H., Villaseñor, A., and Bormann, P. Public release of the  
646 ISC–GEM global instrumental earthquake catalogue (1900–2009). *Seismological Research Letters*, 84(5):810–815, 2013. doi: <https://doi.org/10.1785/0220130034>.  
647
- 648 Tanioka, Y. and Seno, T. Sediment effect on tsunami generation of the 1896 Sanriku tsunami earthquake. *Geophysical Research Letters*, 28  
649 (17):3389–3392, 2001. doi: <https://doi.org/10.1029/2001GL013149>.
- 650 Tanioka, Y., Ruff, L., and Satake, K. What controls the lateral variation of large earthquake occurrence along the Japan Trench? *Island Arc*,  
651 6(3):261–266, 1997. doi: <https://doi.org/10.1111/j.1440-1738.1997.tb00176.x>.
- 652 Titov, V., Rabinovich, A. B., Mofjeld, H. O., Thomson, R. E., and González, F. I. The global reach of the 26 December 2004 Sumatra tsunami.  
653 *Science*, 309(5743):2045–2048, 2005. doi: <https://doi.org/10.1126/science.1114576>.
- 654 Van Rijnsingen, E., Lallemand, S., Peyret, M., Arcay, D., Heuret, A., Funicello, F., and Corbi, F. How subduction interface roughness influ-  
655 ences the occurrence of large interplate earthquakes. *Geochemistry, Geophysics, Geosystems*, 19(8):2342–2370, 2018. doi: <https://doi.org/10.1029/2018GC007618>.  
656
- 657 Van Zelst, I. Data & scripts for ‘Investigating global correlations between tsunami, earthquake, and subduction zone characteristics’, 2022.  
658 <https://doi.org/10.5281/zenodo.7118751>.
- 659 Van Zelst, I., Cramer, F., Pusok, A. E., Glerum, A., Dannberg, J., and Thieulot, C. 101 geodynamic modelling: how to design, interpret, and  
660 communicate numerical studies of the solid earth. *Solid Earth*, 13(3):583–637, 2022. doi: [10.5194/se-13-583-2022](https://doi.org/10.5194/se-13-583-2022).
- 661 von Huene, R., Miller, J. J., Klaeschen, D., and Dartnell, P. A possible source mechanism of the 1946 Unimak Alaska far-field tsunami: uplift  
662 of the mid-slope terrace above a splay fault zone. In *Global Tsunami Science: Past and Future, Volume I*, pages 4189–4201. Springer, 2016.  
663 doi: <https://doi.org/10.1007/s00024-016-1393-x>.
- 664 Waldhauser, F., Schaff, D. P., Diehl, T., and Engdahl, E. R. Splay faults imaged by fluid-driven aftershocks of the 2004 Mw 9.2 Sumatra-  
665 Andaman earthquake. *Geology*, 40(3):243–246, 2012. doi: <https://doi.org/10.1130/G32420.1>.
- 666 Wang, K. and Bilek, S. L. Do subducting seamounts generate or stop large earthquakes? *Geology*, 39(9):819–822, 2011. doi: <https://doi.org/10.1130/G31856.1>.  
667
- 668 Wang, K. and Bilek, S. L. Invited review paper: Fault creep caused by subduction of rough seafloor relief. *Tectonophysics*, 610:1–24, 2014.  
669 doi: <https://doi.org/10.1016/j.tecto.2013.11.024>.
- 670 Wang, Z. and Lin, J. Role of fluids and seamount subduction in interplate coupling and the mechanism of the 2021 mw 7.1 fukushima-oki  
671 earthquake, japan. *Earth and Planetary Science Letters*, 584:117439, 2022. doi: <https://doi.org/10.1016/j.epsl.2022.117439>.
- 672 Wendt, J., Oglesby, D. D., and Geist, E. L. Tsunamis and splay fault dynamics. *Geophysical Research Letters*, 36(15), 2009. doi: <https://doi.org/10.1029/2009GL038295>.  
673
- 674 Yokota, Y., Ishikawa, T., Watanabe, S.-i., Tashiro, T., and Asada, A. Seafloor geodetic constraints on interplate coupling of the Nankai Trough  
675 megathrust zone. *Nature*, 534(7607):374, 2016. doi: <https://doi.org/10.1038/nature17632>.